



Load capacity and fracture modes of instrumented tooth roots under axial compression

Fei Lin^a, Xiqiao Feng^b, Ronald Ordinola-Zapata^c, Bonita VanHeel^d, Alex S.L. Fok^{d,*}

^a Department of Cariology and Endodontology, Peking University School and Hospital of Stomatology & National Center for Stomatology & National Clinical Research Center for Oral Diseases & National Engineering Research Center of Oral Biomaterials and Digital Medical Devices, Beijing 100081, China

^b Institute of Biomechanics and Medical Engineering, Department of Engineering Mechanics, Tsinghua University, Beijing 100084, China

^c Division of Endodontics, Department of Restorative Sciences, School of Dentistry, University of Minnesota, Minneapolis, MN 55455, USA

^d Minnesota Dental Research Center for Biomaterials and Biomechanics, School of Dentistry, University of Minnesota, Minneapolis, MN 55455, USA

ARTICLE INFO

Keywords:

Root canal instrumentation
Load capacity
Tooth root fracture
Finite element analysis

ABSTRACT

Objective: To investigate the influences of root canal instrumentation on the load capacity and fracture modes of tooth roots under axial compression by performing mechanical tests and finite element analysis (FEA).

Methods: Thirty bovine incisor roots were trimmed into cylinders of 5.0 mm diameter. They were randomly divided into two groups, one with root canals instrumented to ~2.0 mm in diameter, and one without instrumentation. The specimens were fractured under uniaxial compression at a crosshead speed of 0.2 mm/min, and then micro-CT was used to reveal the fracture patterns in three dimensions. FEA was further performed, using the extended finite element method (XFEM), to compare the compression-induced stress distributions and the initiation and propagation of root fractures in both groups.

Results: The mean fracture load of the non-instrumented group (2334 ± 436 N) was statistically significantly higher than that of the instrumented group (1857 ± 377 N) ($p < 0.01$). Three types of root fractures were identified according to the path and length of the cracks: end-face crack, partial-length crack, and full-length crack. As to the fracture modes, the incidence of partial-length root fracture was the highest in both groups (60% for the non-instrumented group and 53.3% for the instrumented group), followed by that of full-length fracture (26.7% and 40%, respectively) and then end-face fracture (13.3% and 6.7%, respectively). The percentage of full-length fracture was slightly higher in the instrumented group. FEA showed that the compression induced higher Tresca stresses but lower maximum principal stresses in the canal walls of the instrumented group. The XFEM simulations predicted that the fracture of both groups initiated from the outer root surface near an end face and propagated axially to the middle third of the root and radially towards the root canal. These numerical results agreed well with our experimental findings.

Significance: Within the limitation of this study, it was found that root canal instrumentation could significantly decrease the load capacity of tooth roots and potentially increase their susceptibility to full-length root fracture under uniaxial compression.

1. Introduction

Vertical root fracture (VRF), or longitudinally oriented fracture along the tooth root, has been reported to occur more commonly in endodontically-treated teeth [1], for which root canal instrumentation is performed to remove the infected dentin, bacteria and their byproducts from the canal wall [2]. Currently, the most widely used instruments for root canal preparation are rotary or reciprocating nickel-titanium (Ni-Ti) instruments [3]. A downside of this procedure is the dentinal

wall reduction and, although controversial, instrumentation has also been linked with the creation of dentinal microcracks [1,4]. Furthermore, root canal instrumentation alters the canal's initial oval cross-sectional form; the canal will become more regular and rounded, with a taper that ranges between 4% and 8% [5–8].

The influences of root canal instrumentation on the load capacity and fracture mode of endodontically-treated teeth are still under debate. According to certain laboratory experiments, the structural loss induced by instrumentation weakened the root [9–11], while some others

* Correspondence to: 16-212 Moos Health Science Tower, 515 Delaware Street S.E., Minneapolis, MN 55455, USA.

E-mail address: alexfok@umn.edu (A.S.L. Fok).

<https://doi.org/10.1016/j.dental.2023.08.177>

Received 19 August 2023; Accepted 23 August 2023

Available online 28 August 2023

0109-5641/© 2023 The Academy of Dental Materials. Published by Elsevier Inc. All rights reserved.

demonstrated that the more regular, circular shape of instrumented root canals could reduce the stress concentrations seen at the canal wall [12, 13]. In the previous studies, the role of the occlusal force in the occurrence of VRF and its interaction with root canal instrumentation were rarely addressed. Instead, an internal pressure on the canal wall, which simulates the root canal instrumentation or the insertion of a post, was often introduced to study the load capacity of roots [9,12–15]. The finite element method were also used to simulate the fracture processes of teeth [9,10,13,15,16]. Finite element analysis (FEA) is more informative and reliable when accompanied and validated by experiments [17,18]. Furthermore, the mechanisms of VRF, i.e., crack initiation and propagation, remain elusive. Therefore, it is of considerable interest to systematically investigate the effect of root canal instrumentation on VRF, a topic that is not fully understood in the endodontic field [1].

In this paper, therefore, we combine experimental measurements and FEA to investigate the influences of root canal instrumentation on the load capacity and fracture modes of tooth roots. The null hypothesis was that there existed no significant difference in the load capacity or fracture modes between endodontically-instrumented roots and non-instrumented roots.

2. Materials and methods

2.1. Preparation of specimens

Freshly extracted, single-rooted bovine incisors were used in this study. To minimize the effects of anatomical variations, the crown and root tip of each tooth were resected, and the remaining root was trimmed into a cylinder of 5.0 mm in outer diameter. The specimens were randomly divided into two groups of $n = 15$. In the first group, the root canals remained non-instrumented, while in the second group, the root canals were instrumented to ~ 2.0 mm in diameter.

All the samples were scanned using micro-computed tomography (micro-CT; HMX-XT 225, Nikon Metrology Inc., Brighton, MI, USA) to exclude samples with pre-existing cracks. The micro-CT parameters used were: 20 μm isotropic resolution, 115 kV accelerating voltage, 90 μA tube current, 720 projections, 4 frames/projection, and 708 ms exposure time. The images were reconstructed into three-dimensional structures using the software CT Pro 3D XT 3.1.11 (Nikon Metrology Inc., Brighton, MI, USA). The average cross-sectional area (A) of each specimen over its length was calculated using the image processing software VGSTUDIO MAX 3.1 (Volume Graphics GmbH, Heidelberg, Germany).

The specimens were kept hydrated in distilled water during and after preparation until being tested mechanically.

2.2. Axial compressive loading test

The specimens were loaded with uniaxial compression using a universal testing machine (MTS 858 MiniBionix II, Eden Prairie, MN, USA) at a crosshead speed of 0.2 mm/min until fracture. Fracture was identified from an abrupt drop in load shown in the monitor. The highest load was recorded as the fracture load (F), and the uniaxial fracture stress (σ_f) of each specimen was calculated using the following equation:

$$\sigma_f = \frac{F}{A},$$

where A is the average cross-sectional area of the specimen.

2.3. Fracture analysis using micro-CT

All the fractured specimens were scanned using micro-CT to reveal the crack paths with the same parameters as described above. After reconstruction, the three-dimensional (3D) geometries of the cracks were rendered by post-processing the micro-CT images of the fractured samples using the software Mimics Research 19.0 (Materialise, Leuven,

Table 1

Material properties of root dentin assumed in FEA.

Property	Value	Reference
Young's modulus	18.6 GPa	[31]
Poisson's ratio	0.3	[31]
Tensile strength	108 MPa	[32]
Fracture energy	1.2 N•mm ⁻¹	[33]

Belgium).

2.4. FEA

FEA was performed to first determine the stress distributions in the sample specimens from the two groups. The micro-CT images of these specimens were input into Mimics and 3-Matic (Materialise, Leuven, Belgium) for 3D model construction. Uniform surface meshes and isoparametric tetrahedral elements were used. The meshed models were transferred to Abaqus/CAE (SIMULIA, Dassault Systèmes, Johnston, RI, USA) for the definitions of material properties, loading and boundary conditions. The root dentin was assumed to be homogenous, isotropic, and linearly elastic (Table 1). Two horizontal plates were created, one at the bottom and one at the top, to compress the specimen. The frictional coefficient between the plates and the specimen was set as 0.3. The bottom surface of the bottom plate was fully constrained while the top plate was lowered gradually to apply an axial compressive load to the sample. The maximum load applied was 2000 N, according to the fracture loads recorded in the mechanical test (see later). Convergent tests were conducted with reducing mesh sizes until consistent results had been achieved. The final non-instrumented model had 21070 elements and 5365 nodes, and the final instrumented model had 14977 elements and 4088 nodes. The maximum principal and Tresca (maximum shear) stress distributions were compared between the sample specimens from the two groups.

2.5. Fracture simulation using extended finite element method (XFEM)

XFEM (available in Abaqus) was also used with the same models to simulate crack initiation and propagation in the sample specimens from both groups. Root dentin was considered brittle. Thus, the maximum principal stress criterion was used for crack initiation while the energy-based damage evolution criterion was used for crack propagation [19] (Table 1). No pre-cracks were embedded into the models. An axial compressive load was applied as described above to cause crack initiation and propagation within the root. The site of crack initiation and the direction of crack propagation in the sample specimens from the two groups were compared with each other as well as with the experimental observations.

2.6. Statistical analysis

The sample size was determined using a priori power calculation with software G*Power (Heinrich-Heine-Universität, Düsseldorf, Germany). A pilot study with three samples per group was performed to calculate the mean and standard deviation of the fracture load. The minimum sample size per group was determined to be 9 with a power of 95% and a Type-I error rate of 5%.

Statistical analysis was performed on the fracture loads and fracture stresses using SPSS (SPSS Inc., Chicago, IL, USA). The Kolmogorov-Smirnov and Levene tests were conducted to determine the parametric distribution and homogeneity of variances, respectively. The independent-samples t-test was performed to assess the statistical significance in the differences between the two groups, with $\alpha = 0.05$.

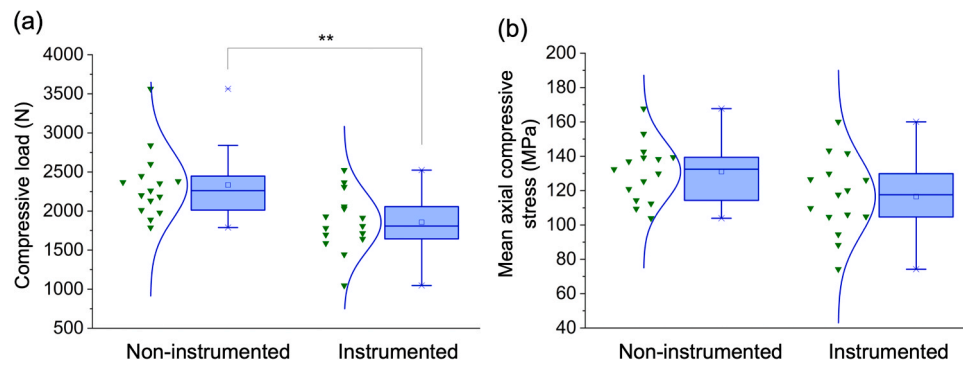


Fig. 1. Compressive load (a) and mean axial compressive stress (b) at fracture of non-instrumented and instrumented groups. ** indicates statistically significant difference.

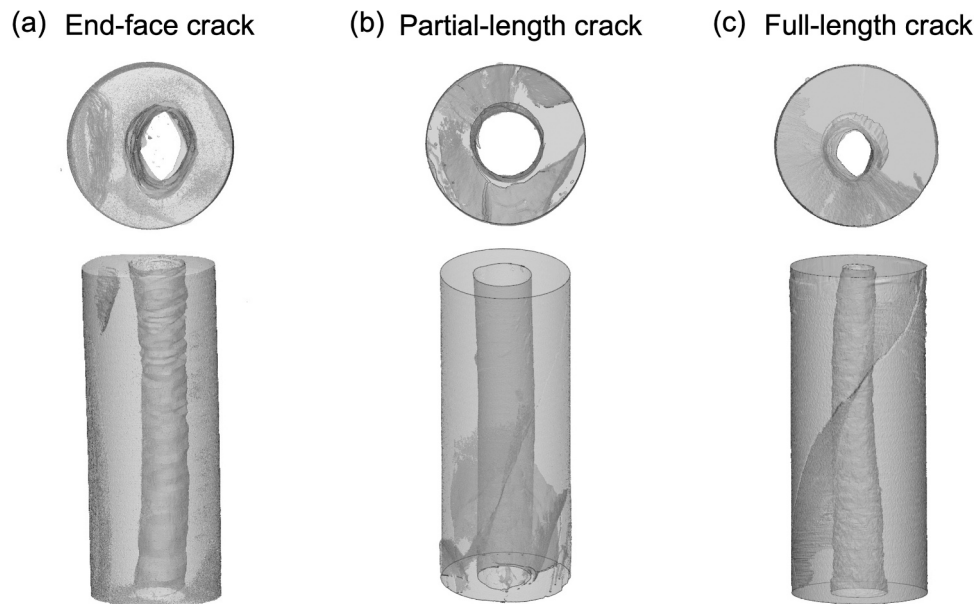


Fig. 2. 3D renditions of fractured specimens with different modes of root fractures. (a) End-face crack: the crack extended from the external surface to the nearest end face without crossing the root canal. (b) Partial-length crack: the crack initiated from the external surface and crossed the root canal while extending obliquely to the nearest end face. (c) Full-length crack: the crack started from one end face, crossed the root canal obliquely and reached the other end face.

3. Results

3.1. Fracture load

The mean fracture loads of the non-instrumented and instrumented groups were 2334 ± 436 N and 1857 ± 377 N, respectively. The difference between the two groups was statistically significant ($p < 0.01$, Fig. 1a).

3.2. Fracture stress

The mean compressive fracture stresses of the non-instrumented and instrumented groups were 131.08 ± 17.24 MPa and 116.52 ± 22.58 MPa, respectively. There was no statistically significant difference between the two groups ($p > 0.05$, Fig. 1b).

3.3. Fracture analysis

Three types of root fracture could be identified (Fig. 2), which all appeared to contain shear cracks lying at $\sim 45^\circ$ with respect to the vertical axis but of different lengths:

Table 2

Proportions of the three types of root fractures in the non-instrumented group and instrumented group (n = 15).

	Non-instrumented group	Instrumented group
End-face crack	13.3% (2)	6.7% (1)
Partial-length crack	60% (9)	53.3% (8)
Full-length crack	26.7% (4)	40% (6)

- (i) *End-face crack*: The crack extended from the external surface to the nearest end face without crossing the root canal (Fig. 2a).
- (ii) *Partial-length crack*: The crack extended from the external surface and crossed the root canal while extending obliquely to the nearest end face (Fig. 2b).
- (iii) *Full-length crack*: The crack extended from one end face, crossed the root canal obliquely and reached the other end face (Fig. 2c).

The 3D renditions of the three types of root fracture described above are shown in Fig. 2. Among them, the partial-length crack was the most common in both groups, followed by the full-length crack and then the end-face crack (Table 2). The percentage of full-length cracks was slightly higher in the instrumented group. More than one cracks lying at

Table 3

Mean fracture loads (N) of the three types of root fractures in the non-instrumented group and instrumented group (n = 15).

	Non-instrumented group	Instrumented group
End-face crack	1952 ± 87	1587
Partial-length crack	2263 ± 292	1809 ± 415
Full-length crack	2686 ± 617	1966 ± 353

different angles were observed in some specimens.

The mean fracture load of specimens with full-length cracks was the highest in both groups, followed by that of specimens with partial-length cracks and then that of specimens with end-face cracks (Table 3). The non-instrumented group showed a higher mean fracture load in all 3 types of root fracture.

According to the micro-CT images of the fractured specimens, the end-face cracks initiated from the outer surface of the root and propagated obliquely towards the nearest end face, leading to chipping (Figs. 3a and 4a). The partial-length cracks also seemed to initiate from the outer root surface. However, they propagated more inwardly and crossed the root canal (Figs. 3b and 4b). Different from the other two types of cracks, the full-length cracks seemed to have initiated from the canal wall (Figs. 3c and 4c). They also propagated more longitudinally, crossing the root canal before reaching the far end face.

3.4. Stress distributions in root dentin

Under a load of 2000 N, the peak maximum principal stress in the non-instrumented sample was 17 MPa and located beneath the top surface of the specimen. In the instrumented sample, the peak maximum principal stress was 30 MPa and located at the top surface of the

specimen. There were greater tensile stress concentrations on the canal wall of the non-instrumented sample compared with that of the instrumented sample (Fig. 5).

The peak Tresca stress was 161 MPa in the non-instrumented sample, located at the bottom surface. In the instrumented sample, it was 258 MPa and located at the top surface. The instrumented sample showed higher Tresca stresses along the entire root (Fig. 5). The canal wall, especially at the upper-middle and lower-middle thirds of the root, exhibited greater Tresca stresses, particularly in the instrumented sample.

3.5. Numerical prediction of cracks

XFEM predicted that the cracks in both samples initiated from the outer root surface beneath the top end face (Fig. 6a). The cracks first propagated axially downwards to the middle third of the root before turning obliquely towards the canal wall. The 3D renditions of the corresponding fractured specimens (Fig. 6b) were compared with the models predicted by XFEM. It can be seen that the main crack of each fractured specimen was located roughly at the same position as that predicted by XFEM. However, both actual specimens exhibited more cracks than the models, and the actual main cracks were slightly more vertical.

4. Discussions

VRF has been shown to be associated with multiple factors, including the external root morphology, the root canal curvature, the thickness of the proximal dentinal wall, the pressure from lateral compaction, etc. [9, 12–15]. In the present study, cylindrical specimens, not conical roots, were used for fracture testing to minimize the effect of anatomical

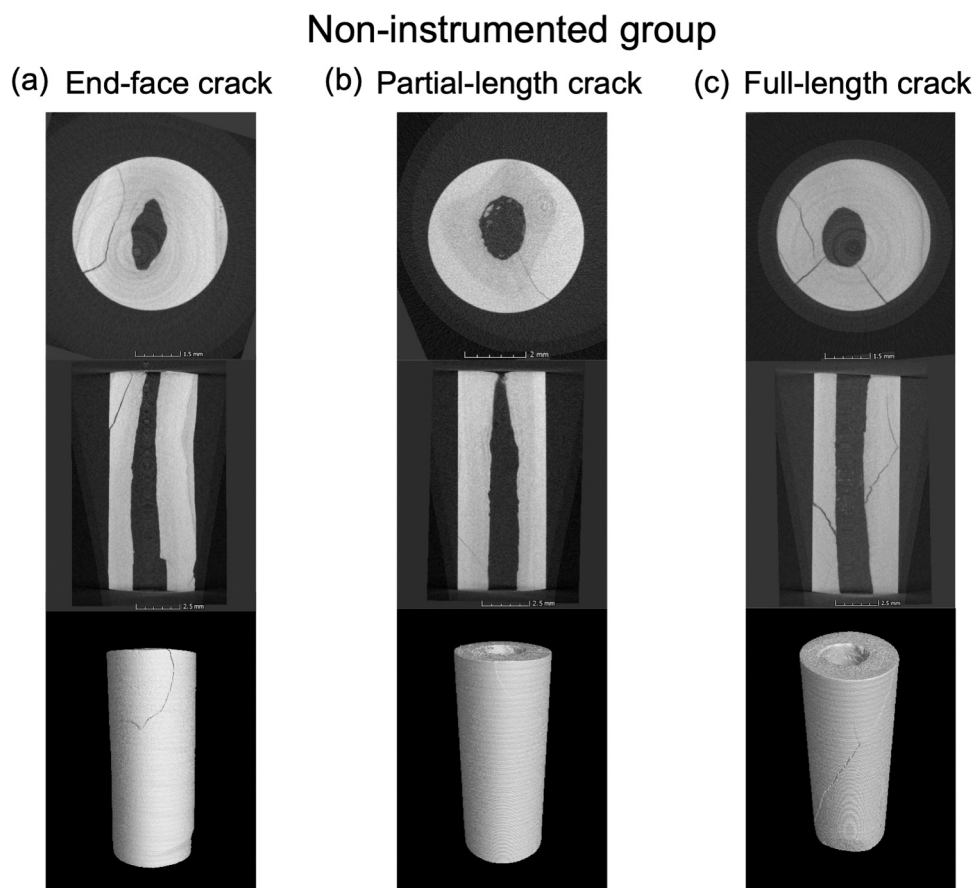


Fig. 3. Specimens from non-instrumented group with end-face crack (a), partial-length crack (b), and full-length crack (c).

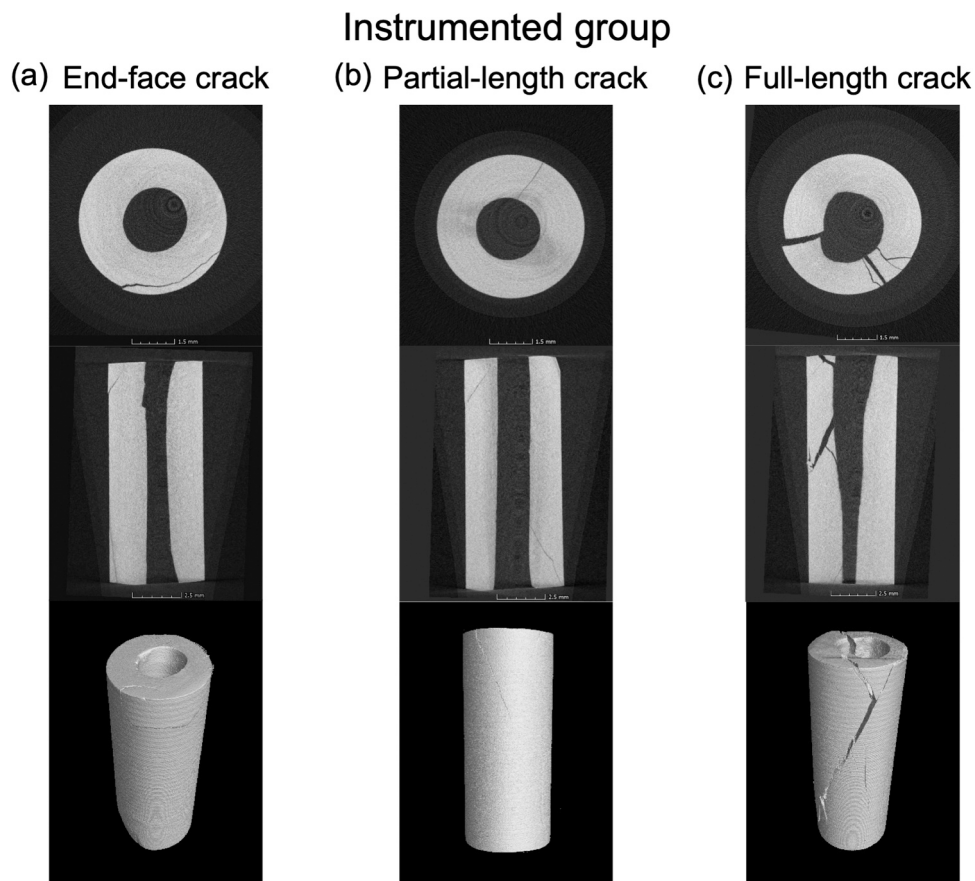


Fig. 4. Specimens from instrumented group with end-face crack (a), partial-length crack (b), and full-length crack (c).

variations. Hollow brittle cylinders and their failure behaviors under axial compression have been widely studied in engineering to understand, e.g., the fracture mechanisms of rocks and concrete as supporting structures [20–22]. So far, however, the human tooth root – also a hollow structure under axial compression – has been rarely studied using similar methods to understand its fracture mechanisms.

Human tooth roots are tapered hollow cylindrical structures with oval cross-sections. In real life, they are surrounded by the periodontal ligament and bone which help to distribute the load more evenly over their height. In laboratory tests, however, the small root tip would develop high stress concentrations under loads and fail predominantly, especially in the absence of supporting materials to simulate the surrounding bone. This would conceal the influence of root canal morphology on the stress distribution or load capacity of tooth roots. With a more regular geometry, the hollow cylindrical specimens used in the present study could avoid premature failure at the root tip, thus allowing the effect of instrumentation on the load capacity of tooth roots to be studied properly.

The instrumented group presented lower fracture loads and a higher incidence of full-length root fracture. The lower fracture loads could be attributed to the greater stresses as a result of the reduced cross-sectional area after instrumentation [23,24]. This is supported by other studies which demonstrated that root canal instrumentation led to higher stresses at the radicular level [9,10,25]. For example, Sathorn et al. reported that, under internal pressure, the removal of root dentine increased tensile stress concentrations both on the canal wall and on the outer root surface [9].

However, some other studies demonstrated that root canal enlargement did not reduce the load capacity of teeth [26]. It was reported that the more circular and regular root canals after instrumentation could eliminate the asymmetrical stress concentrations seen in

non-instrumented irregular root canals [9]. This was also found in the present study (Fig. 5), but our specimens showed a reduction in the load capacity by root canal enlargement. The result is probably dependent on the type of loading. Still, it is worth pointing out that, as stress concentrations can divert a crack path, their reduction in the instrumented group may explain the higher incidence of full-length root fracture in this group.

For isotropic brittle materials, the cracking direction is usually normal to the most tensile principal stress. The cracks appeared to initiate from the position of the peak maximum principal stress near one of the two end faces (Fig. 6). Theoretically, under uniaxial compression, no tensile principal stress is expected. However, the end faces of a specimen were constrained in the lateral directions because of friction while the bulk of the cylinder expanded radially due to the Poisson's ratio effect. This mismatch in radial expansion would create tensile hoop stresses near the end faces. Cracks initiated by these stresses are likely to be axial and radial. Bending due to eccentric deformation of the cylinder because of the irregular root canal may also have contributed tensile stresses, especially on the root canal wall (Fig. 5). However, these bending stresses are along the axial direction and thus the cracks they initiate tend to be along the horizontal direction.

The specimen was subjected to uniaxial compression with the maximum shear stress lying at planes 45° to the vertical axis. These seemed to be the main planes of crack propagation (Fig. 6), which are similar to the shear bands observed in ductile metals and quasi-brittle materials under uniaxial compression [27]. However, the fracture surfaces of brittle or quasi-brittle materials are rough and are hard to slide against each other under compression. Thus, under uniaxial compression, the cracks in these materials tend to seek a more vertical crack path with smaller frictional resistance, as found in the present study (Fig. 6). Note that the frictional interaction between opposing crack faces was

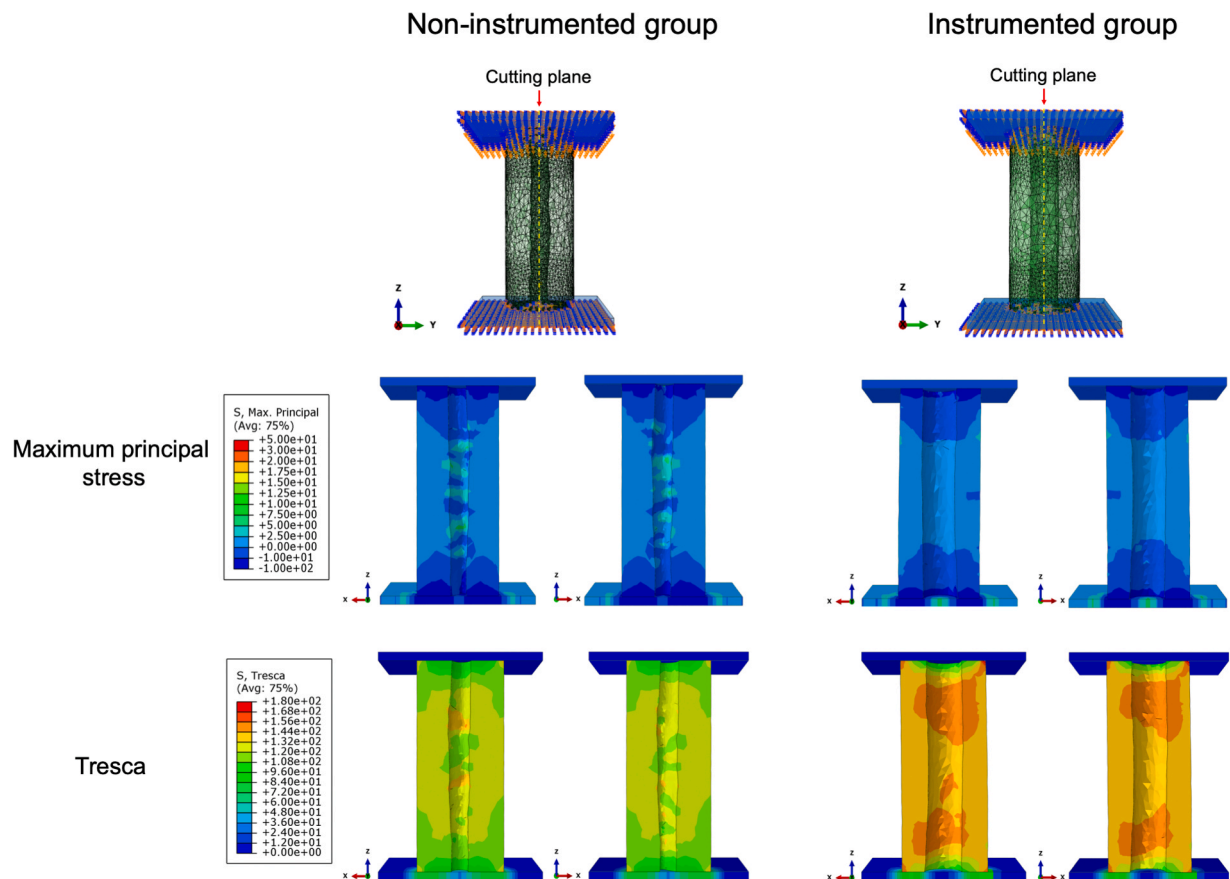


Fig. 5. Maximum principal and Tresca stress distributions on cross sections of opposing halves in non-instrumented and instrumented specimens.

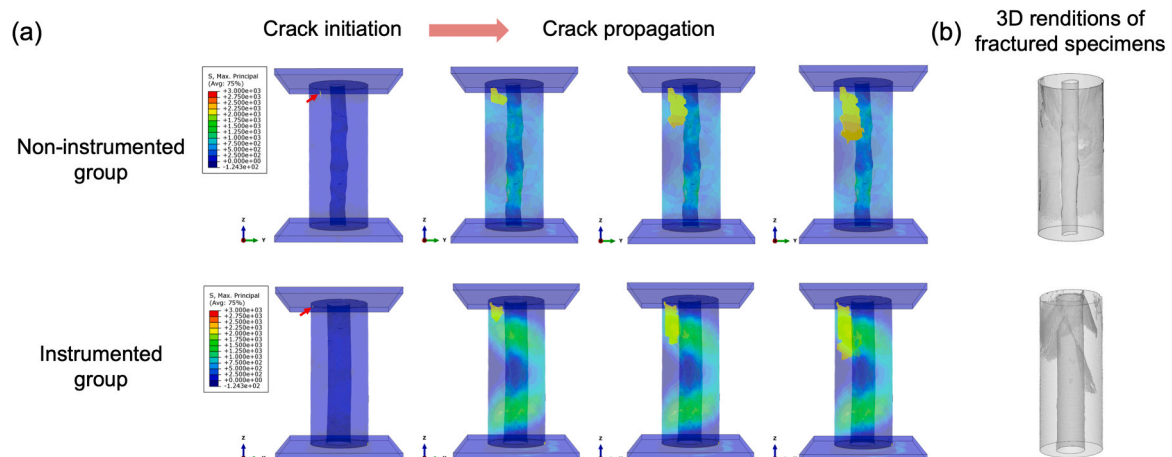


Fig. 6. (a) Crack initiation (red arrows) and propagation (yellow regions) predicted using XFEM in non-instrumented and instrumented specimens. (b) 3D renditions of corresponding fractured specimens for comparison.

not considered in the XFEM analysis. As a result, the predicted crack paths were closer to the 45° planes.

From the perspective of micromechanics, the root dentin of a tooth, like most brittle materials, contains preexisting microcracks, weak interfaces, or voids. Theoretically, under uniaxial compression, high tensile and shear stresses could be induced at the tip of the microcracks under a combination of closure and frictional sliding of the microcrack faces [28]. For brittle materials, these stresses would cause kinking of the microcracks and eventually drive them to propagate in the same direction as the compression [28]. Clinically, not all observed VRFs

propagate vertically as root dentin is not purely brittle. The complex masticatory forces and the constraint of the tooth root imposed by the surrounding alveolar bone might also be reasons for the slant cracks observed.

In this study, we divide the root fracture into three types, according to whether the crack, which started from one end, crossed the root canal or extended to the other end (Fig. 7). Clinically, a vertical crack that involves the root canal would subsequently lead to crack contamination and bone resorption. In contrast, a tooth with a root crack that does not involve the root canal may have a better chance of survival. Even a tooth

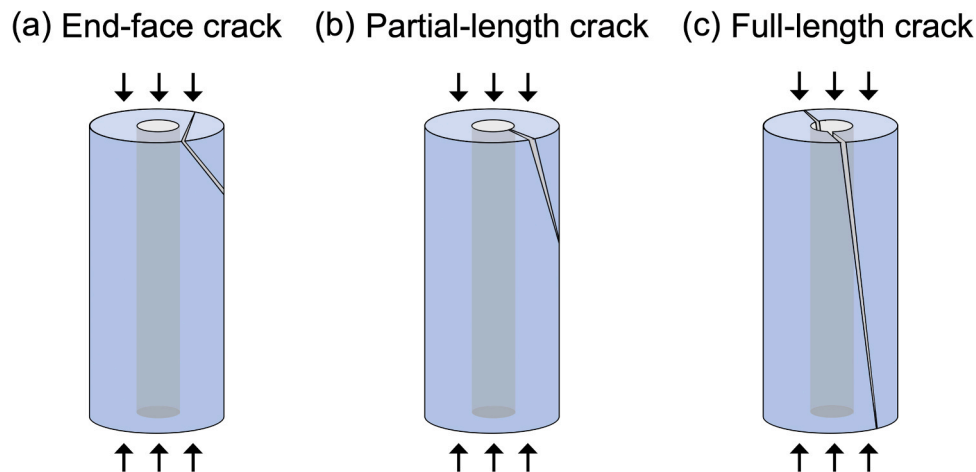


Fig. 7. Schematic diagrams of three types of root fracture. (a) End-face crack. (b) Partial-length crack. (c) Full-length splitting crack. The black arrows indicate the applied compressive force.

with a partial-length root crack may possibly survive if the crack is located at the apical third of the root and there is no bacterial involvement. To the best of our knowledge, this was the first time that such an experiment–FEA combined approach had been applied in the dental field for evaluating the fracture behavior of tooth roots.

The present study found that full-length cracks were slightly more prevalent in the instrumented group, indicating that endodontically-instrumented teeth might be more prone to devastating VRF. In contrast, the occurrence of end-face cracks was slightly higher in the non-instrumented group, suggesting that non-endodontically-instrumented teeth are more likely to fracture with short and localized cracks. This may explain why VRFs are infrequent in untreated teeth. However, the small number of end-face cracks should be noted. Most of the samples from both groups exhibited partial-length cracks, formed by the dominating shear stresses. The multiple fractures seen in some of the specimens might be induced by such reasons as distributed defects in the samples. Clinically, VRFs may also present partial-length cracks along the longitudinal direction, even though their prevalence is unclear. Few studies consider the etiology or formation mechanisms of these partial-length cracks. The present study indicated that the compressive occlusal load may be a contributing factor to these root fractures.

Clinically, VRF mostly starts from the canal wall and is more common in endodontically-treated teeth [1,15,29]. Although many of the specimens from the non-instrumented group had cracks initiated from the outer root surface, probably due to tensile stresses generated by the end-face constraint, as explained above, the main driving force for crack propagation, which determined the final crack shape, was the shear stress. Indeed, the FEA showed greater shear stresses around the canal wall, especially in the instrumented group.

VRFs are not confined to endodontically-treated teeth [30]. Although it is a rare event, a clinical study reported that VRF could also occur in non-endodontically-treated teeth from excessive or repetitive masticatory forces [30]. However, the initiation sites of these VRFs were not mentioned. The present study showed that, using a compressive load that mimic the actual vertical occlusal forces, fractures similar to VRFs could also be created in the non-instrumented group.

Future studies using the methodology presented in this work should aim to produce more clinically-representative VRFs by, for example, minimizing the end-face constraints of the tooth roots.

5. Conclusions

Within the limitation of this study, it was shown that root canal instrumentation could significantly decrease the load capacity of tooth roots and potentially increase their susceptibility to full-length fracture

under uniaxial compression. The null hypothesis was therefore rejected. The fracture behavior of tooth roots could be studied using the experimental–numerical hybrid approach presented in this work. In particular, XFEM could accurately predict the initiation and propagation of longitudinal root fracture.

Acknowledgment

This work was supported by a National Natural Science Foundation of China grant (No. 12102009) awarded to Fei Lin. Fei Lin would also like to acknowledge the Minnesota Dental Research Center for Biomaterials and Biomechanics for awarding her a Key-Opinion-Leader (KOL) scholarship, sponsored by 3Mgives, and for hosting her visit during which this study was performed.

References

- [1] Patel S, Bhuva B, Bose R. Present status and future directions: vertical root fractures in root filled teeth. *Int Endod J* 2022;55:804–26.
- [2] Usman N, Baumgartner JC, Marshall JG. Influence of instrument size on root canal debridement. *J Endod* 2004;30:110–2.
- [3] Bürklein S, Arias A. Effectiveness of root canal instrumentation for the treatment of apical periodontitis: a systematic review and meta-analysis. *Int Endod J* 2022: 1–27.
- [4] Heberer MT, Roggendorf HC, Faber FJ, Lawrenz NA, Frankenberger R, Roggendorf MJ. Longitudinal craze line propagation in human root dentin after instrumentation with NiTi rotary files of different instrument tapers after long-term chewing simulation. *Clin Oral Invest* 2022;26:2671–9.
- [5] Wu MK, Wessellink PR. A primary observation on the preparation and obturation of oval canals. *Int Endod J* 2001;34:137–41.
- [6] Bryant ST, Thompson SA, Al-Omari MAO, Dummer PMH. Shaping ability of Profile rotary nickel-titanium instruments with ISO sized tips in simulated root canals: Part 1. *Int Endod J* 1998;31:275–81.
- [7] Wu MK, R'oris A, Barkis D, Wessellink PR. Prevalence and extent of long oval canals in the apical third. *Oral Surg Oral Med Oral Pathol Oral Radio Endod* 2000;89: 739–43.
- [8] Paqué F, Balmer M, Attin T, Peters OA. Preparation of oval-shaped root canals in mandibular molars using nickel-titanium rotary instruments: a micro-computed tomography study. *J Endod* 2010;36:703–7.
- [9] Sathorn C, Palamara JEA, Palamara D, Messer HH. Effect of root canal size and external root surface morphology on fracture susceptibility and pattern: a finite element analysis. *J Endod* 2005;31:288–92.
- [10] Yuan K, Niu C, Xie Q, Jiang W, Gao L, Ma R, et al. Apical stress distribution under vertical compaction of gutta-percha and occlusal loads in canals with varying apical sizes: a three-dimensional finite element analysis. *Int Endod J* 2018;51: 233–9.
- [11] Munari LS, Bowles WR, Fok ASL. Relationship between canal enlargement and fracture load of root dentin sections. *Dent Mater* 2019;35: 818–24.
- [12] Sathorn C, Palamara JEA, Messer HH. A comparison of the effects of two canal preparation techniques on root fracture susceptibility and fracture pattern. *J Endod* 2005;31:283–7.
- [13] Lertchirakarn V, Palamara JEA, Messer HH. Patterns of vertical root fracture: factors affecting stress distribution in the root canal. *J Endod* 2003;29:523–8.

- [14] Pilo R, Metzger Z, Brosh T. Effect of root morphology on the susceptibility of endodontically treated teeth to vertical root fracture: An ex-vivo model. *J Mech Behav Biomed Mater* 2017;69: 267–74.
- [15] Lertchirakarn V, Palamara JEA, Messer HH. Finite element analysis and strain-gauge studies of vertical root fracture. *J Endod* 2003;29:529–34.
- [16] Chen G, Fan W, Mishra S, El-Atem A, Schuetz MA, Xiao Y. Tooth fracture risk analysis based on a new finite element dental structure models using micro-CT data. *Comput Biol Med* 2012;42:957–63.
- [17] Ordinola-Zapata R, Lin F, Nagarkar S, Perdigão J. A critical analysis of research methods and experimental models to study the load capacity and clinical behaviour of the root filled teeth. *Int Endod J* 2022;55: 471–94.
- [18] Lin F, Ordinola-Zapata R, Ye N, Xu H, Fok ASL. Fatigue analysis of restored teeth longitudinally cracked under cyclic loading. *Dent Mater* 2022;38: 204–13.
- [19] Zhang Z, Thompson M, Field C, Li W, Li Q, Swain MV. Fracture behavior of inlay and onlay fixed partial dentures - An in-vitro experimental and XFEM modeling study. *J Mech Behav Biomed Mater* 2016;59: 279–90.
- [20] Yang SQ. Fracturing mechanism of compressed hollow-cylinder sandstone evaluated by X-ray Micro-CT scanning. *Rock Mech Rock Eng* 2018;51: 2033–53.
- [21] Li Z, Zhou H, Jiang Y, Hu D, Zhang C. Methodology for establishing comprehensive stress paths in rocks during hollow cylinder testing. *Rock Mech Rock Eng* 2019;52: 1055–74.
- [22] Wang Y, Han JQ, Song ZY, Zhu C. Macro-meso failure behavior of pre-flawed hollow-cylinder granite under multi-level cyclic loads: Insights from acoustic emission and post-test CT scanning. *Eng Fract Mech* 2021;258:108074.
- [23] Ossareh A, Rosentritt M, Kishen A. Biomechanical studies on the effect of iatrogenic dentin removal on vertical root fractures. *J Conserv Dent* 2018;21: 290–6.
- [24] Akhlaghi NM, Bajgiran LM, Naghdi A, Behrooz E, Khalilak Z. The minimum residual root thickness after using ProTaper, RaCe and Gates-Glidden drills: a cone beam computerized tomography study. *Eur J Dent* 2015;9: 228–33.
- [25] Smoljan M, Hussein MO, Guentsch A, Ibrahim M. Influence of progressive versus minimal canal preparations on the fracture resistance of mandibular molars: a 3-dimensional finite element analysis. *J Endod* 2021;47:932–8.
- [26] Bagheri R, Abbaszadegan A, Nabavizadeh MR, Ferooz M, Parashos P. Mathematical validation of measurement of root fracture resistance: an in vitro study. *BMC Oral Health* 2021;21:1–5.
- [27] Yu W, Li X, Zhang J, Hou S, Lv Y. Dynamic deformation behavior and fracture characteristics of a near α TA31 titanium alloy at high strain rates. *Mater* 2022;15.
- [28] Yu SW, Feng XQ. A micromechanics-based damage model for microcrack-weakened brittle solids. *Mech Mater* 1995;20:59–76.
- [29] Zou X, Liu D, Yue L, Wu M. The ability of cone-beam computerized tomography to detect vertical root fractures in endodontically treated and nonendodontically treated teeth: a report of 3 cases. *Oral Surgery. Oral Med Oral Pathol Oral Radio Endodontology*. 2011;111:797–801.
- [30] Chan CP, Tseng SC, Lin CP, Huang CC, Tsai TP, Chen CC. Vertical root fracture in nonendodontically treated teeth - a clinical report of 64 cases in Chinese patients. *J Endod* 1998;24:678–81.
- [31] Rees JS, Jacobsen PH. The elastic moduli of enamel and dentine. *Clin Mater* 1993; 14:35–9.
- [32] Yan J, Taskanak B, Mecholsky JJ. Fractography and fracture toughness of human dentin. *J Mech Behav Biomed Mater* 2009;2:478–84.
- [33] Arola D, Reprogl RK. Effects of aging on the mechanical behavior of human dentin. *Biomaterials* 2005;26:4051–61.